

# Average Quasar Spectra in the Context of Eigenvector 1<sup>1</sup>

J. W. Sulentic<sup>2†</sup>, P. Marziani<sup>3†</sup>, R. Zamanov<sup>3†</sup>, R. Bachev<sup>2,3†</sup>, M. Calvani<sup>3†</sup>, D. Dultzin-Hacyan<sup>4†</sup>

## ABSTRACT

Recent work has shown that it is possible to systematize quasar spectral diversity in a parameter space called “Eigenvector 1” (E1). We present median AGN spectra for fixed regions of the E1 (optical) parameter space (FWHM( $H\beta$ ) vs. equivalent width ratio  $R_{\text{FeII}}=W(\text{FeII } \lambda 4570)/W(H\beta)$ ). Comparison of the median spectra for different regions show considerable differences. We suggest that an E1-driven approach to median/average spectra emphasizes significant differences between AGN, and offers more insights into AGN physics and dynamics than a single population median/average derived from a large and heterogeneous sample of sources. We find that the  $H\beta$  broad component line profile changes in shape along the E1 sequence both in average centroid shift and asymmetry. While objects with  $\text{FWHM}(H\beta_{\text{BC}}) \lesssim 4000 \text{ km s}^{-1}$  are well fitted by a Lorentz function, AGN with  $\text{FWHM}(H\beta_{\text{BC}}) \gtrsim 4000 \text{ km s}^{-1}$  are well fitted if two broad line components are used: a broad (the “classical” broad line component) and a very broad/redshifted component.

*Subject headings:* quasars: emission lines – quasars: general – galaxies: active

## 1. Introduction

Studies of broad emission line spectra for AGN provide both the strongest constraint on models for the nebular physics and kinematic models of the broad line emitting clouds. Ideally one would like to have both high signal-to-noise ratio (S/N) and moderate resolution ( $\lesssim 5 \text{ \AA}$ ) measures for the strongest high and low ionization lines as well as measures across as wide a wavelength range as possible in order to better characterize the continuum shape. The former measures have

---

<sup>0†</sup> “Northern Quasar Alliance”

<sup>1</sup>Based in part on data collected at ESO La Silla.

<sup>2</sup>Department of Physics and Astronomy, University of Alabama, Tuscaloosa, AL 35487, USA

<sup>3</sup>Osservatorio Astronomico di Padova, Vicolo dell’Osservatorio 5, I-35122 Padova, Italy

<sup>4</sup>Instituto de Astronomía, UNAM, Apdo. Postal 70-264, 04510 Mexico D.F., Mexico

led to the Eigenvector 1 parameter space concept (Sulentic et al. 2000a,b) that is, in part, built upon foundations laid almost ten years ago (Boroson & Green 1992; hereafter BG92). The above goals are very observing time intensive but recent AGN surveys have provided an alternate method for examining quasar spectra from 1000 – 10000 Å. Average or composite spectra derived from large survey databases involving hundreds of AGN (LBQS: Francis et al. 1991; HST: Zheng et al. 1997; 1998; FIRST: Brotherton et al. 2001; Sloan survey: Vanden Berk et al. 2001) make it possible to generate a “typical” quasar spectrum from blueward of Ly $\alpha$  to H $\alpha$ .

What is unclear is whether such composite spectra are astrophysically useful beyond, perhaps, allowing us to identify lines that are too weak to be seen in individual source spectra. The fundamental question is whether the similarities or the differences in AGN line and continuum phenomenology tell us more about the underlying physics. The Eigenvector 1 concept has been advanced as a possible “H-R Diagram” for AGN in the sense that it appears to provide parameter space discrimination between all major classes of broad line sources as well as a correlation for, at least, radio quiet sources (Sulentic et al. 2000b). The correlation and distribution of radio-quiet sources (with  $\text{FWHM}(\text{H}\beta) \leq 4000 \text{ km s}^{-1}$ ) in E1 have been reasonably well fit with a model that sees accretion rate, convolved with source orientation, as the principal physical driver (Marziani et al. 2001). The generality of E1, of course, requires much further testing but unless it is far off the mark, it suggests that average or composite spectra should be viewed in the same way that one would view an average stellar spectrum taken over the full effective temperature range that is observed in the H-R Diagram (spectral types O-M). Interpretation of composite spectra from heterogeneous samples will be complicated in two ways: (1) they will be subject to selection biases dependent on the relative number of sources with each “spectra type” in a given sample and, more significantly, (2) they will average the spectra of sources with dramatically different physical properties. We suggest that the most useful approach to averaging AGN spectra lies within the E1 context. We present average spectra for fixed domain quadrants in E1 followed by a brief discussion of important differences. The emphasis is on the  $\text{FWHM}(\text{H}\beta)$  measures although large differences in the equivalent width parameter are also seen. Full discussion of the equivalent width differences must wait for significant numbers of very high S/N measures for  $\text{FeII}_{\text{opt}}$  weak sources.

## 2. Sample, Data Reduction and Analysis

Our current sample includes optical spectra for 187 sources obtained between 1988 and 1996. They cover the wavelength range that includes H $\gamma$ , H $\beta$ , and most of the optical  $\text{FeII}_{\text{opt}}$  emission (4200-5700 Å in the rest frame). Spectra were obtained with the following telescopes and spectrographs: ESO 1.5m (B&Ch), San Pedro Martir 2.2m (B&Ch), Calar Alto 2.2m (B&Ch), KPNO 2.2m (Gold), and Mount Ekar (Asiago) 1.82m (B&Ch). Data for 52 objects can be found

in Marziani et al. (1996) and the unpublished part of the dataset will appear in a forthcoming paper (Marziani et al. 2002). Spectra were taken with very similar instrumental setups including typically 120Å/mm dispersion and 2 arcsec slit width yielding resolution in the range 4-7 Å FWHM. The S/N is typically in the range  $\approx 20$ -30. Spectra with  $S/N \lesssim 10$  were excluded. The sample includes spectra for 187 type 1 AGN with redshifts  $z \lesssim 0.8$ ,  $m_V \lesssim 16$ . Table 1 summarizes the properties of our data sample within the context of Eigenvector 1 (see §3.1 for bin definition). Composite spectra were obtained by taking the median of all spectra with 1Å binning. The S/N of the composite spectra was  $\gtrsim 100$  except for bin A3 where only 5 objects were available, and  $S/N \approx 50$ . No composite spectra were obtained for the rare objects in the outlier domain ( $FWHM(H\beta_{BC}) \gtrsim 4000$  km s $^{-1}$  and  $R_{FeII} \gtrsim 0.5$ ) which spans several E1 bins.

The following analysis procedures were applied to each spectrum (see Marziani et al. 1996 for details). (1) Deredshifting using the narrow line component of  $H\beta$ , and/or  $[OIII]\lambda 4959,5007$  as rest frame measures. (2) Normalization using the best estimate for a local continuum at  $\lambda \approx 5100$  Å. (3) Subtraction of FeII  $\lambda 4570$  emission blends using a template based on the spectrum of IZw1 which also yielded the FeII blend equivalent width  $W(FeII \lambda 4570)$ . (4) Subtraction of the  $[OIII]\lambda 4959,5007$  and HeII  $\lambda 4686$  lines. (5) Subtraction of the narrow component from  $H\beta$  ( $H\beta_{NC}$ ) using a Gaussian model. In cases where no clear inflection between broad and narrow components was seen, two alternative approaches were employed: (a) we assumed that  $FWHM(H\beta_{NC}) \approx FWHM([OIII]\lambda 5007)$  or (b) we assumed that  $FWHM(H\beta_{BC}) \approx FWHM(FeII \lambda 4570)$ . The latter approach was useful for Narrow Line Seyfert 1 sources. Following these procedures we extracted  $H\beta_{BC}$  and derived equivalent width and FWHM measures which allowed us to populate E1. Host galaxy contamination was not significant for the luminous AGN included in this sample. The typical uncertainty for  $FWHM(H\beta_{BC})$  is about 10% and for  $W(H\beta_{BC})$  and  $W(FeII \lambda 4570)$  about 10-15%. Errors on  $R_{FeII}$  are estimated to be less than 0.2.

### 3. Results

#### 3.1. Spectral Types

The distribution of 187 sources in the optical E1 plane ( $FWHM(H\beta_{BC})$  vs.  $R_{FeII}$ ) is shown in Figure 1. We binned the optical parameter plane as shown in Figure 1 and as defined in Table 1. The bins were arbitrarily set to constant  $\Delta FWHM(H\beta_{BC}) = 4000$  km s $^{-1}$ , and  $\Delta R_{FeII} = 0.5$ . A finer subdivision is not warranted at this time by the accuracy of the measures or the heterogeneity of the data sample. The adopted A-B bin labeling reflects our earlier suggestion that two distinct radio-quiet AGN populations may exist: Pop. A (“pure” radio-quiet) and Pop. B (same as the radio-loud domain; see Table 1). The numeral accompanying the letter designation for A

bins reflects the increasing strength of  $R_{\text{FeII}}$ . The “+” designations for B bins reflect increasing  $\text{FWHM}(\text{H}\beta_{\text{BC}})$ . There are many measures that distinguish between radio-quiet Pop. A and B as defined with a boundary at  $\text{FWHM}(\text{H}\beta_{\text{BC}}) \approx 4000 \text{ km s}^{-1}$ . There are also many measures that support a phenomenological commonality between population B and radio-loud sources (Sulentic et al. 2000a,b,c). Table 1 summarizes the properties of domain space bins that are occupied by a significant number of sources. The composite (median) spectra after processing step 2 (continuum normalized) and after step 3 ( $\text{FeII}_{\text{opt}}$  subtracted) are presented in the left and right panels of Figure 2 respectively. The median spectra are available in digital format on the World Wide Web.<sup>6</sup>

It is important to note that the E1 binned median spectra are unlikely to be strongly influenced by any luminosity dependence since: (a) there is, so far, no convincing evidence for a difference in line profile properties with source redshift/luminosity (Sulentic et al. 2000a) and (b) for any sub-sample,  $\Delta M_B \lesssim 1.5 \lesssim \sigma_{M_B}$  (see Table 1). It is also worth noting that the median  $M_B$  of our sources is close to the limit separating Seyfert 1 galaxies and quasars ( $M_B = -23.0$ ). This should not be considered a particular problem because there is no discontinuity in the AGN luminosity distribution. Radio-loud sources in our sample show a higher mean luminosity perhaps due to the inclusion of many beamed sources but Pop. B radio-quiet sources, co-spatial with them in E1, are not more luminous than Pop. A radio-quiet sources.

Our  $W(\text{FeII } \lambda 4570)$  uncertainty estimate (§2) is valid if  $\text{FeII } \lambda 4570$  is clearly detected above the noise. However, the minimum  $W(\text{FeII } \lambda 4570)$  for which it is possible to visually detect  $\text{FeII } \lambda 4570$  depends both on S/N and on  $\text{FeII } \lambda 4570$  FWHM. For  $S/N \approx 20$ , upper limits for  $\text{FeII } \lambda 4570$  detection is estimated to be  $\approx 14, 17, 20 \text{ \AA}$  for  $\text{FWHM} = 2500, 5000, 7500 \text{ km s}^{-1}$  respectively. The utility of the composite spectra is also evident because of the much higher S/N in bins B1 (and B1<sup>+</sup>), which contain many upper limits because  $\text{FeII } \lambda 4570$  is intrinsically weak in Population B sources. In those bins it is possible to obtain more reliable  $W(\text{FeII } \lambda 4570)$  measurements from composite spectra.

### 3.2. Median $\text{H}\beta_{\text{BC}}$ Profiles Across E1

Median spectra of the  $\text{H}\beta_{\text{BC}}$  profile are shown in Fig. 3. They were extracted from the median spectra after  $\text{FeII}_{\text{opt}}$  and continuum subtraction to take advantage of the much higher S/N of the composites spectra. We derived a pure  $\text{H}\beta_{\text{BC}}$  profile by first subtracting  $[\text{OIII}]\lambda 4959, 5007$  and  $\text{HeII}\lambda 4686$  and then fitting  $\text{H}\beta_{\text{BC}}$  with a high-order spline function to avoid the effects of finite S/N and to interpolate across the  $\text{H}\beta_{\text{NC}}$ . This approach has proven to be successful for measuring

---

<sup>6</sup>At the address <http://panoramix.pd.astro.it/~marziani/medians.zip>

line parameters in noisier line profiles (Marziani et al. 1996). It is preferable to template fitting because it makes no assumptions about the shape of the profile. Table 1 presents  $\text{FWHM}(\text{H}\beta_{\text{BC}})$  as well as line centroids at 1/2 and 1/4 maximum intensities derived from the median spectra. The median  $\text{H}\beta_{\text{BC}}$  profiles in Pop. A are almost symmetric with a slight blueward asymmetry in bin A2. The blue asymmetry becomes visually apparent in bin A3 which contains sources that are extreme in many ways. Table 1 shows that the profiles of NLSy1 do not differ from bin A1 and A2 median spectra. The smaller median  $\text{FWHM H}\beta_{\text{BC}}$  reflects an arbitrary cutoff ( $\leq 2000 \text{ km s}^{-1}$ ) in the definition of NLSy1s.

The profiles of Pop. A sources are very different from those of Pop. B. The median profiles of population B sources are red asymmetric with the strongest asymmetry in the (few) bin  $\text{B1}^{++}$  sources. The different shape may point towards different BLR structure/kinematics in these sources. Profile shape was not selected *a priori* in the population definition that was based on a possible  $\text{FWHM}(\text{H}\beta_{\text{BC}})$  break. An alternate way to describe profile asymmetry involves fitting a functional form to the median profiles. The  $\text{H}\beta_{\text{BC}}$  profile in NLSy1 sources is well fit by a Lorentz function (see also Véron-Cetty, Véron, & Gonçalves 2001). The same is generally true for A1 and A2 median profiles while A3  $\text{H}\beta_{\text{BC}}$  is based on only five sources.

A Lorentzian function is definitely not a satisfactory description for bin B median profiles. The  $\text{H}\beta_{\text{BC}}$  profile is significantly different and this can be seen even in Fig. 2. The profile becomes more Gaussian but we were unable to fit bin B profiles with any simple and physically meaningful function. The best fits to  $\text{H}\beta_{\text{BC}}$  bin B1 and B1+ profiles required the sum of two Gaussians: (1) a  $\text{FWHM} \approx 4000\text{-}5000 \text{ km s}^{-1}$  unshifted Gaussian core and (2) a broader  $\text{FWHM} \approx 10000 \text{ km s}^{-1}$  redshifted ( $\Delta v_r \sim 1000 \text{ km s}^{-1}$ ) Gaussian base. The main difference between B1 and B1+ may be related to the strength of the “very broad component”. We will show in the next section: (1) that many radio-loud and some radio-quiet Pop. B sources show unambiguous very broad components and (2) that the interpretation of the profile in terms of two components may have a straightforward physical meaning.

## 4. Discussion

We find significant and systematic differences in median spectra across E1.  $\text{FWHM}(\text{H}\beta_{\text{BC}})$  and  $\text{R}_{\text{FeII}}$  both show systematic changes and the other E1 parameters reinforce this dichotomy (pop. A sources show a systematic blueshift of the  $\text{CIV } \lambda 1549$  broad line profile and a soft X-ray excess while pop. B source do not: Sulentic 2000ab). Pop. A sources show a more symmetric profile with the largest  $\text{R}_{\text{FeII}}$  values (indicating large  $\text{W}(\text{FeII } \lambda 4570)$  and somewhat depressed  $\text{W}(\text{H}\beta_{\text{BC}})$ ). As one enters the population B domain the radio-loud source fraction increases.  $\text{H}\beta_{\text{BC}}$  becomes increasingly broad and red asymmetric for both radio-loud and radio-quiet sources. Over-

all NLSy1/Pop. A spectra show lower ionization spectra than Pop. B (Marziani et al. 2001). Comparison between high ( $\text{CIV}\lambda 1549_{\text{BC}}$ : HIL) and low ( $\text{H}\beta_{\text{BC}}$ : LIL) ionization emission lines suggests that they are emitted in disjoint regions in pop. A. Contrarily, both LIL and HIL may arise from a single region in Pop. B sources (Marziani et al. 1996; Sulentic et al. 2000a,b). It is more accurate to say that we cannot rule out the possibility that both HIL and LIL arise from the same line emitting regions (broad and very broad) in population B (Sulentic 2000a). The  $\text{H}\beta_{\text{BC}}$  profile analysis indicates that the BLR – and specifically the region emitting the low ionization lines – is most probably structurally different in Population A and Population B sources. It is beyond the scope of the present paper to report on detailed model calculation. We note however that the Lorentz profile is consistent with emission from an extended accretion disk. This reinforces the suggestion that the LIL spectra in Pop. A sources arise from a disk. The situation is less clear for Pop. B sources where the Eddington ratio may be much lower. There is good evidence that sometimes only one of the two emission components is present in Pop. B sources (pure BLR or pure VBLR; see Sulentic et al. 2000c). In a companion paper, we suggest that even the Narrow Line Region structure/kinematics may be changing along the E1 sequence (Zamanov et al. 2002).

#### 4.1. The Very Broad Line Region Issue

Can the double Gaussian model that is needed to fit Pop. B (and radio-loud) profiles be physically justified? Several lines of evidence point towards the existence of a Very Broad Line Region (VBLR) at the inner edge of the BLR (Corbin 1997a,b). Emission from this region may be thought of as a sort of inner, large covering factor, “boundary layer” where gas begins to become optically thick (Marziani & Sulentic 1993; Sulentic et al. 2000c). In objects like the luminous quasar PG 1416-129, almost pure VBLR emission survived after a continuum intensity decrease effectively quenched the classical BLR. 3C232 (Marziani et al. 1996) may represent a good radio-loud analog of PG1416. Other examples of possible pure VBLR line sources can be found in Sulentic et al. 2000c.  $\text{HeII}\lambda 4686$  has also been known for some time to show a profile systematically broader than  $\text{H}\beta$  in some sources (see Osterbrock & Shuder 1982) and this can be seen in Figure 2. Unfortunately  $\text{HeII}\lambda 4686$  is usually weak and/or blended with stronger  $\text{H}\beta$  and  $\text{FeII}$  emission (it is on the red end of  $\text{FeII}\lambda 4570$ ). Detection of the  $\text{HeII}\lambda 4686$  broad component is therefore a function of  $\text{FeII}_{\text{opt}}$  strength and S/N. The strongest very broad  $\text{HeII}\lambda 4686$  feature is seen in the bin A1 median spectrum where we have a favorable combination of S/N,  $\text{H}\beta$  width,  $\text{FeII}_{\text{opt}}$  weakness and  $\text{HeII}\lambda 4686$  strength. The latter bias reflects the inclusion of data from an observing run dedicated to studying strong  $\text{HeII}\lambda 4686$  emission. A very broad  $\text{HeII}\lambda 4686$  profile is sometimes seen in pop. A sources (e.g. Ton S 180) with much narrower  $\text{FeII}\lambda 4570$ . However, in I Zw 1, the highest S/N spectra fail to detect any trace of  $\text{HeII}\lambda 4686$  emission. At this time the question of  $\text{HeII}\lambda 4686$  emission must be considered on an object-by-object basis. We note that  $\text{HeII}\lambda 4686$  strength was

an orthogonal (eigenvector 2) parameter in the principal component analysis of Boroson & Green (1992).

## 5. Conclusion

We generated average QSO spectra in the 4200–5700 Å spectral region for fixed optical parameter bins in E1. In fixed parameter range bins the mean spectral type appears to change systematically across E1. This systematic behaviour is reflected in E1 X-ray and UV measures as well. Composite spectra in an E1 context should provide useful input for theoretical modeling. Ignoring the diversity of the AGN  $H\beta_{BC}$  profile may make any theoretical modeling of the BLR kinematics and dynamics unreliable.

The authors acknowledge support from the Italian Ministry of University and Scientific and Technological Research (MURST) through grant and Cofin 00–02–004.

## REFERENCES

- Boroson T.A., Green R.F., 1992, ApJS, 80, 109
- Brotherton, M. S., Tran, H. D., Becker, R. H., Gregg, M. D., Laurent-Muehleisen, S. A., & White, R. L. 2001, ApJ, 546, 775
- Corbin, M. R. 1997a, ApJS, 113, 245
- Corbin, M. R. 1997b, ApJ, 485, 517
- Francis, P. J., Hewett, P. C., Foltz, C. B., Chaffee, F. H., Weymann, R. J., & Morris, S. L. 1991, ApJ, 373, 465
- Marziani, P. & Sulentic, J.W. 1993, ApJ, 409, 612
- Marziani, P., Sulentic, J. W., Dultzin-Hacyan, D., Calvani, M., & Moles, M. 1996, ApJS, 104, 37
- Marziani, P., Sulentic, J. W., Zwitter, T., Dultzin-Hacyan, D., & Calvani, M. 2001, ApJ, 558, 553
- Osterbrock, D. E. & Shuder, J. M. 1982, ApJS, 49, 149
- Sulentic J.W., Marziani P., Dultzin-Hacyan D., 2000a, AR A&A, 38, 521
- Sulentic, J. W., Zwitter, T., Marziani, P., & Dultzin-Hacyan, D. 2000b, ApJ, 536, L5

- Sulentic, J. W., Marziani, P., Zwitter, T., Dultzin-Hacyan, D., & Calvani, M. 2000c, *ApJ*, 545, L15
- Vanden Berk D.E., Richards G.T., Bauer A., et al., 2001, astro-ph/0105231
- Véron-Cetty, M.-P., Véron, P., & Gonçalves, A. C. 2001, *A&A*, 372, 730
- Zheng, W., Kriss, G. A., Telfer, R. C., Grimes, J. P., & Davidsen, A. F. 1997, *ApJ*, 475, 469
- Zheng, W., Kriss, G. A., Telfer, R. C., Grimes, J. P., & Davidsen, A. F. 1998, *ApJ*, 492, 855



Table 1. Sample Properties

Type	$R_{\text{FeII}}$	$\text{FWHM}(\text{H}\beta_{\text{BC}})$ [km s <sup>-1</sup> ]	$N_{\text{obj}}$	$N_{\text{RL}}$	$M_B^{\text{a}}$	$\sigma_{M_B}$	$\overline{\text{FWHM}(\text{H}\beta_{\text{BC}})}^{\text{b}}$ [km s <sup>-1</sup> ]	$\overline{R_{\text{FeII}}}$	$\overline{c(1/2)}^{\text{b},c}$ [km s <sup>-1</sup> ]	$\overline{c(1/4)}^{\text{b},c}$ [km s <sup>-1</sup> ]	Best Fit
Total	all	all	187	64	-23.7	2.0	...	0.37	...	...	...
NLSy1	all	$\leq 2000$	24	2	-23.0	1.7	1500	0.61	40	0	Lorentz
Pop A <sup>d</sup>	all	$\leq 4000$	80	11	-23.3	1.8	2300	0.49	20	30	Lorentz
A3	1.0 – 1.5	0 – 4000	5	0	-24.5	2.2	2350	1.23	-280	-290	Lorentz
A2	0.5 – 1.0	0 – 4000	26	3	-23.3	1.5	1950	0.70	-20	-30	Lorentz
A1	0.0 – 0.5	0 – 4000	49	6	-23.2	1.8	2250	0.31	30	250	Lorentz
Pop B <sup>e</sup>	all	$>4000$	97	50	-24.2	2.0	5700	0.22	200	700	Double Gaussian
B1	0.0 – 0.5	4000 – 8000	76	35	-24.2	2.0	5600	0.23	250	700	Double Gaussian
B1 <sup>+</sup>	0.0 – 0.5	8000 – 12000	17	12	-24.1	2.1	10000	0.17	270	1700	Double Gaussian
B1 <sup>++</sup>	0.0 – 0.5	$>12000$	4	3	...	...	...	...	...	...	...
outliers	$>0.5$	$>4000$	10	3	-23.0	2.3	...	0.80	...	...	...

<sup>a</sup>Absolute B magnitude from the Véron-Cetty and Véron Catalogue, for  $H_0 = 50 \text{ km s}^{-1} \text{ Mpc}^{-1}$ ,  $q_0 = 0$ .

<sup>b</sup>Values measured on a high order spline function representative of the  $\text{H}\beta_{\text{BC}}$  of each median spectrum.

<sup>c</sup>Centroid at fractional intensity  $\frac{i}{2}$  are defined as  $c(i/4) = (\lambda_B + \lambda_R - 2\lambda_0)/\lambda_0$ , where  $\lambda_0 = 4861.33 \text{ \AA}$ , and  $\lambda_B$  and  $\lambda_R$  are the wavelength of the blue and red line side at the given fractional intensity.

<sup>d</sup>Pop. A  $\equiv \text{A1} \cup \text{A2} \cup \text{A3}$ .

<sup>e</sup>Pop. B  $\equiv \text{B1} \cup \text{B1}^+ \cup \text{B1}^{++}$ , with outliers (O) excluded

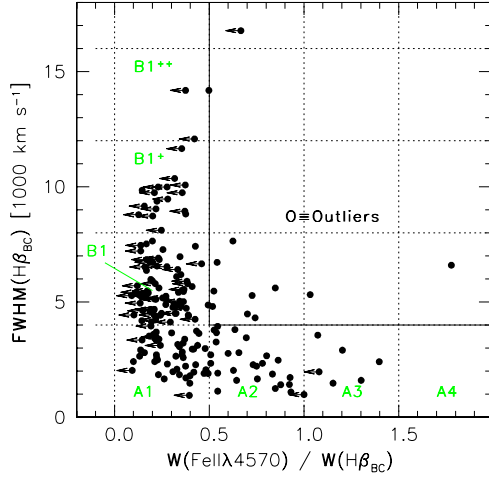


Fig. 1.— The optical parameter plane ( $R_{\text{FeII}}$ - $\text{FWHM}(\text{H}\beta_{\text{BC}})$ ) of Eigenvector 1. This is the largest sample that yet displayed in an E1 context. Dotted lines correspond to the borders between different spectral types also listed in Table 1. The abscissa is  $R_{\text{FeII}} = W(\text{FeII } \lambda 4570) / W(\text{H}\beta_{\text{BC}})$ . The thin solid line indicates the boundary of “outlier” sources and is, so far, a zone of avoidance in quasar parameter space. Horizontal arrows denote FeII  $\lambda 4570$  upper limits. Note that upper limits dominate single  $R_{\text{FeII}}$  measurements in the B1 and B1<sup>+</sup> domains, while the higher S/N ratio of the median spectra allow for a more accurate determination.

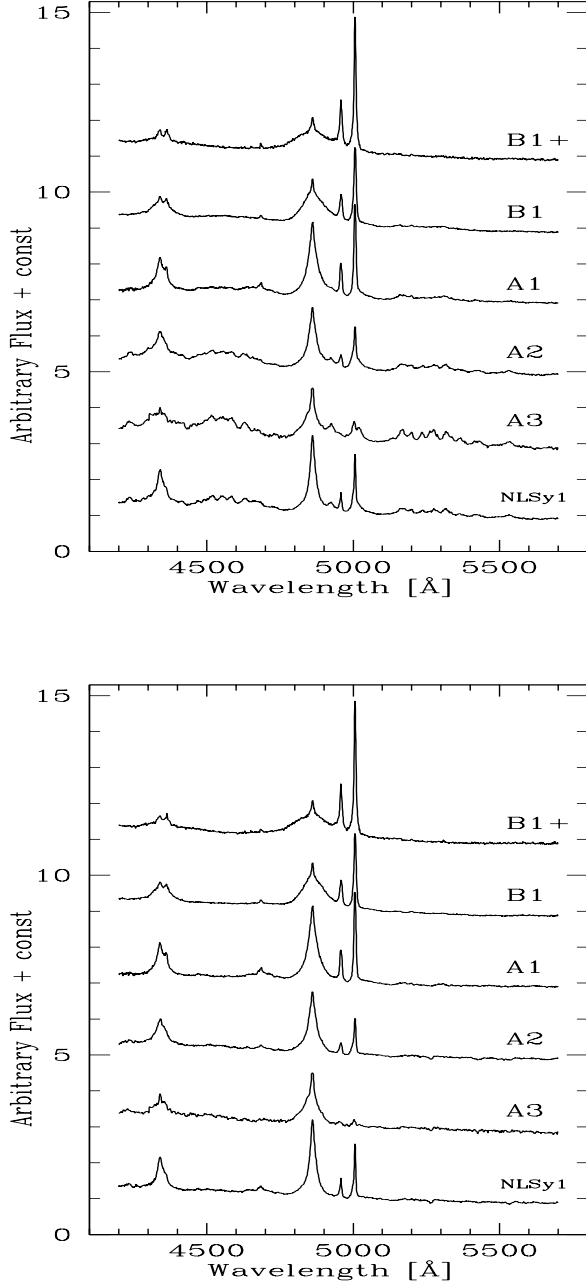


Fig. 2.— Left panel: Composite (median) spectra of the E1 parameter bins defined in Table 1 and Figure 1. Right panel: the same composite spectra with FeII<sub>opt</sub> emission subtracted.

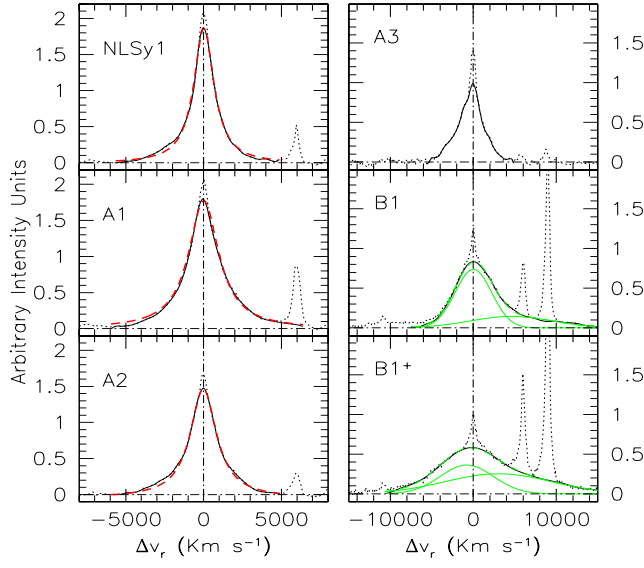


Fig. 3.—  $\text{FeII}_{\text{opt}}$ , and continuum subtracted  $\text{H}\beta$  composite line profiles for the different E1 parameter bins defined in Figure 1. Solid lines show the profile  $\text{H}\beta_{\text{BC}}$  after subtraction of narrow line emission components. A Lorentzian fit (dashed line) is superimposed on the NLS1, A1, A2 profiles. The individual components of a double Gaussian (thin lines) and resultant fit (dashed line) are shown for B1 and B1<sup>+</sup>.